Marked changes in electron transport through the blue copper protein azurin in the solid state upon deuteration

Nadav Amdursky[a,b], Israel Pecht[c], Mordechai Sheves[b,1], and David Cahen[a,1]

Departments of [a]Materials and Interfaces, [b]Organic Chemistry, and [c]Immunology, Weizmann Institute of Science, Rehovot 76100, Israel

Edited by Harry B. Gray, California Institute of Technology, Pasadena, CA, and approved November 27, 2012 (received for review June 21, 2012)

Measuring solid-state electron transport (ETp) across proteins allows studying electron transfer (ET) mechanism(s), while minimizing solvation effects on the process. ETp is, however, sensitive to any static (conformational) or dynamic (vibrational) changes in the protein. Our macroscopic measurements allow extending ETp studies to low temperatures, with the concomitant resolution of lower current densities, because of the larger electrode contact areas. Thus, earlier we reported temperature-independent ETp via the copper protein azurin (Az), from 80 K until denaturation, whereas for apo-Az ETp was temperature dependent above 180 K. Deuteration (H/D substitution) may provide mechanistic information on the question of whether the ETp involves H-bonds in the solid state. Here we report results of kinetic deuterium isotope effect (KIE) measurements on ETp through holo-Az as a function of temperature (30–340 K). Strikingly, deuteration changed ETp from temperature independent to temperature dependent above 180 K. This H/D effect is expressed in KIE values between 1.8 (340 K) and 9.1 (≤180 K). These values are remarkable in light of the previously reported inverse KIE on ET in Az in solution. We ascribe the difference between our KIE results and those observed in solution to the dominance of solvent effects in the latter (larger thermal expansion in H_2O than in D_2O), whereas in our case the KIE is primarily due to intramolecular changes, mainly in the low-frequency structural modes of the protein caused by H/D exchange. The observed high KIE values are consistent with a transport mechanism that involves through-H-bonds of the β-sheet structure of Az, likely also those in the Cu coordination sphere.

protein monolayer | tunneling | current-voltage

The blue copper protein, azurin (Az), functions as an electron carrier in the bacterial energy conversion system (1, 2). The intramolecular electron transfer (ET) reactions in Az in solution have been studied extensively over the last decades by a variety of methods (3–7). In particular, the ET process between the disulfide radical, $RSSR^-$, and the Cu(II) center, or between one of the histidines that was Ru-labeled and the Cu(II) center, has been studied by pulse radiolysis (3) or flash-quench (4, 5) techniques, respectively. More recently, measurements of electron transport (ETp) across Az in the solid state have been made, mostly by scanning probe techniques (8, 9). We have previously reported results of macroscopic ETp measurements via Az and showed that this process is temperature independent down to 80 K (i.e., with no measurable thermal activation barrier) (10, 11). Three types of structural elements were considered in ET pathways in proteins (2, 12): covalent bonds, H-bonds, and through-space jumps. Exploring different pathways of ET in Az by computational algorithms (2) showed that H-bonds are as important as covalent ones for electron tunneling within the protein. The importance of H-bonds was also demonstrated by conductance measurements through peptide monolayers, by either changing the peptide length (13) or by denaturation (14). To assess the impact of H-bonding on the ETp through Az, we now examined its kinetic H/D isotope effect (KIE). We focused on its temperature dependence, because the remarkable temperature independence, exhibited by ETp via protium Az, may provide a sensitive way for interpreting the KIE, because any deviation from this temperature-independent behavior will be discerned.

The deuterium KIE on the ET between the $RSSR^-$ and the Cu (II) center process of Az in solution has previously been studied as a function of temperature (15). Interestingly, it was found that the deuterium KIE is <1 (k_H/k_D = 0.7 at 298 K), and this "inverse" KIE was interpreted as the result of increased negative activation entropy for the ET reaction in the protein in H_2O, compared with that in D_2O. The "inverse" KIE was therefore explained as being a result of differences in the ET driving force, caused by Az undergoing a slightly larger thermal expansion in H_2O than in D_2O (15). Although not discussed in that report (15), the solvent effect on the donor–acceptor electronic coupling may also appear as a change in the activation entropy. The effect of the solvent on the KIE of the redox mechanism of Az was confirmed by Chi et al. (16). They measured the KIE on the electrochemical ET rate between the Cu ion of Az to a gold electrode through an alkanethiol bridge and concluded that their result was mainly due to the solvent effect. Solid-state measurements allow focusing more on the intramolecular ETp, by eliminating solvent effects that were shown to have a crucial effect on the process (15, 16). Indeed, as shown below, we find that the deuterium KIE on the ETp process is very different from that observed previously in solution and thus supports the notion that ETp through H-bonds is significant in the ETp process (2, 12).

Results

An earlier published protocol was used for Az deuteration (15). The extent of the protein's deuteration was determined by NMR. Fig. S1 shows the 1D-NMR spectra of protium- and deuterium-labeled Az. Examination of the amide bond region (at 7.5–9.5 ppm) indicates that the majority of these groups were fully deuterated. Additional protons in the protein might have also undergone deuteration (such as those of the imidazole ring of histidine residues), but these are not clearly observed in the NMR spectra. Comparing the other parts of the NMR spectra shows strong similarity between the protonated and deuterated samples. This indicates that the protein's structural parameters did not change significantly upon deuteration. To further examine the structural similarity between the two samples, we used additional spectroscopic techniques (Fig. 1). The CD spectra (Fig. 1*A*) are identical, showing that the deuterated protein retains its secondary structure of mainly β-sheets, which is consistent with previous results (17). Furthermore, the UV-Vis absorption of the charge transfer band of the Cu(II) (625 nm) and the

Author contributions: N.A., I.P., M.S., and D.C. designed research; N.A. performed research; N.A., I.P., M.S., and D.C. analyzed data; and N.A., I.P., M.S., and D.C. wrote the paper.

The authors declare no conflict of interest.

This article is a PNAS Direct Submission.

[1]To whom correspondence may be addressed. E-mail: mudi.sheves@weizmann.ac.il or david.cahen@weizmann.ac.il.

This article contains supporting information online at www.pnas.org/lookup/suppl/doi:10.1073/pnas.1210457110/-/DCSupplemental.

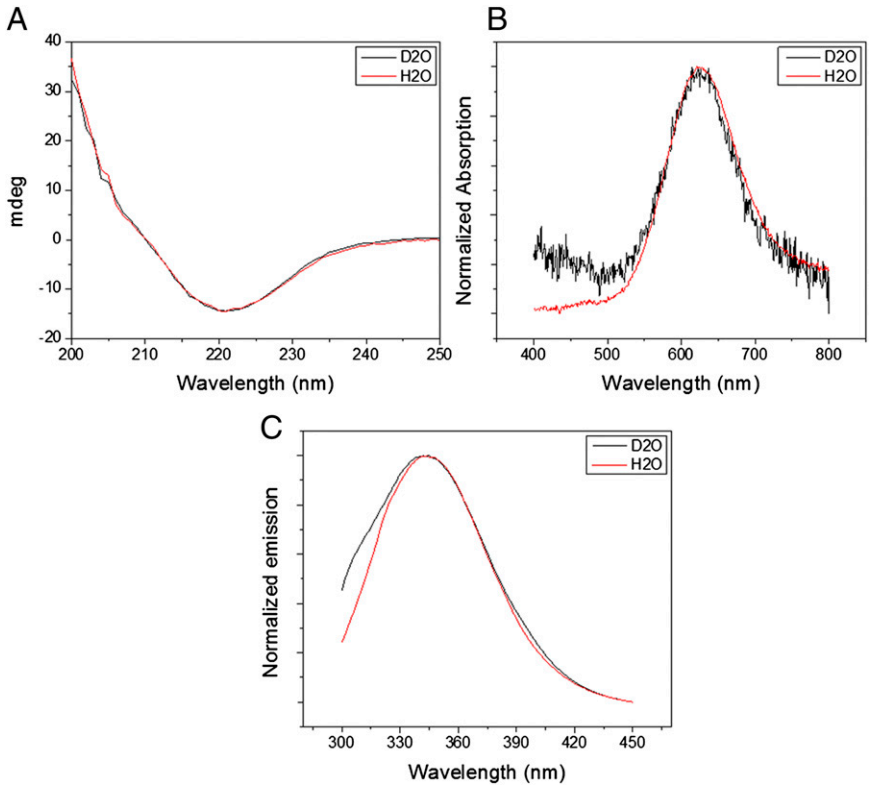

Fig. 1. Spectroscopic analysis of the structure. (*A*) CD, (*B*) UV-Vis, and (*C*) photoluminescence spectra of protium- and deuterium-labeled azurin (red and black curves, respectively).

photoluminescence properties of the single tryptophan residue of Az (Fig. 1 *B* and *C*, respectively), which are also sensitive to the protein conformation, are not affected by deuteration, in agreement with the CD results.

Our earlier described method was used to form monolayers of Az on conductive Si surfaces (10, 11). Both the deuterated and protium-labeled Az surfaces yielded layers with similar ellipsometry-derived optical thickness of 18 Å. This value is approximately half that expected for a monolayer. However, as we explained earlier, this is what is expected for a monolayer, if we consider both the >90% coverage and the voids between the proteins, that are resolved by atomic force microscopy (AFM) topography (18). The AFM topography (Fig. 2*A*) indicated similar morphology and roughness (Fig. 2*A*, *Inset*) of the protium and deuterium samples.

The current-voltage (*I-V*) characteristics of the surfaces were measured with an Hg drop as a second contact (in addition to the conductive Si substrate contact), with a 0.2-mm^2 geometrical contact area. Use of such large area contact yields proportionally higher currents than, for example, use of a nanoscopic area as with scanning probe techniques. The higher currents allow measuring some 7 orders of magnitude smaller current densities, a critical issue for low-temperature measurements. The measurements are made without significant change in the force applied on the sample, in contrast to scanning probe and most other methods that measure samples under compressive or tensile stress.

Comparing the room temperature (298 K) current-voltage, *I-V* curves between deuterated and protium-labeled Az shows that the current density through protium-labeled Az is higher than that through deuterated Az (Fig. 2*B*), yielding a KIE value of 2.4 ± 0.4 (measured at –0.05 V), in contrast to the <1 value measured for Az in solution for intramolecular ET from the $RSSR^-$ radical to the Cu(II) (KIE = 0.7) (15) (Table 1). In the present solid-state measurements only the tightly bound water molecules that help maintain the native conformation remain, essentially eliminating the solvation effects but leaving the intramolecular ones. The relatively high observed KIE suggests that the hydrogen-bonding network of the β-sheet array that supports the protein's structure, and that is affected by deuteration, plays a role in the ETp through (i.e., the "conductivity" of) the protein, as will be discussed below.

Temperature-dependent ETp measurements were carried out between 30 and 340 K. Fig. 3*A* shows the current density through the protein (measured at –0.05 V) as a function of 1,000/T. For protium Az these results extend the range of temperature-independent ETp down to 30 K [i.e., temperatures more than twice lower than what we reported earlier (10)] (compare Fig. 3*A*). Strikingly, we find for deuterated Az two regimes, a temperature-independent one (≤180 K) and a thermally activated one (190–340 K, Fig. 3*B*). The temperature dependence for ETp of the deuterated protein leads to a gradually increasing KIE (Fig. 3*C*) from 1.8 ± 0.3 at high temperature (340 K) to 9.1 ± 1.1 in the low-temperature regime (≤180 K), in sharp contrast to the temperature-independent ETp observed for protium Az (Table 1). The change of the current density of the deuterated sample, as a function of temperature, from a thermally activated regime at high temperatures to a temperature-independent regime at low temperatures, qualitatively resembles the behavior of apo-Az (Fig. 3*D*) (10), as discussed further below.

To verify that the observed effect is indeed a protein-related one, we conducted the same experiment with a thin Au pad as a top contact instead of an Hg drop (Fig. S2). The Au pad was brought into contact by using the lift-off, float-on method (19) and yields similar *I-V* characteristics as those obtained with an Hg drop (11). Au as a top contact allows reaching higher temperatures than Hg, temperatures that are needed to observe the effect of the proteins' denaturation on the ETp magnitude. As we reported earlier for protium-Az (10), a sharp irreversible decrease in the current density is observed at 360 K. By using Au as a top contact we also observed a similar drop in current density of the

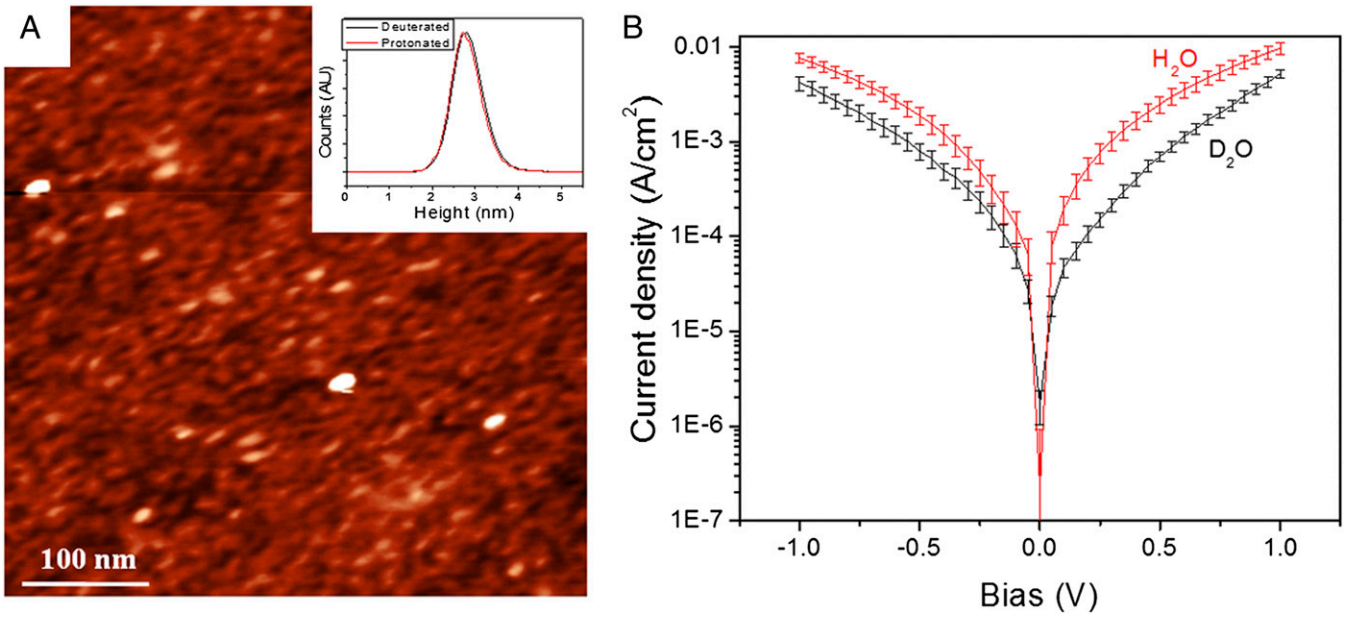

Fig. 2. Surface morphology and current-voltage. (*A*) AFM image of Az coated surface. The z-scale is 7 nm. (*Inset*) Superimposed histogram of the surface roughness of the protium and deuterated Az surfaces. (*B*) Current density vs. voltage at room temperature of protium- and deuterium-labeled Az surfaces.

deuterated Az at a similar temperature (Fig. S2), along with the same temperature-dependent behavior as observed with Hg as top contact, indicating that the observed ETp behavior is indeed related to the protein itself.

Discussion

Origins of KIE in ET. The KIE on ET was observed to be between 1 and 3 and is due mostly to changes in the barrier for electron tunneling upon H/D exchange (20–22), which can be either distinct solvation effects of the proteins in H_2O and D_2O (20, 23–25) or intramolecular changes in the physicochemical properties of the molecule.

The solvation KIE is mainly due to a difference in the Marcus' solvent reorganization energy, λ. This arises from differences in the static dielectric constant, D_s, and refractive index, n, where $\lambda \propto n^{-2}$ ($\propto D_{op}^{-1}$, where D_{op} is the optical dielectric constant) - D_s^{-1} (26, 27). Because these differences between H_2O and D_2O are small (28, 29), only a minor solvent isotope effect is expected (20).

The intramolecular contributions stem from the contribution of H-based vibrational modes, which according to the non-adiabatic ET rate constant, k_{ET}:

$$k_{ET} = \frac{2\pi}{\hbar} H_{D-A}^2 (FC) \qquad [1]$$

can yield two distinct contributions:

i) H/D-based changes in the skeletal vibrational frequencies, which are high-frequency modes and affect H_{D-A}, the electronic coupling between D (donor) and A (acceptor). The specific high-frequency modes [which for amine group protons are in the range of 1,000–1,200 cm^{-1} (30)] are associated with the proton's position and affect the H_{D-A} (31).

ii) The difference in the contributions of low-frequency vibrational modes to the Franck-Condon factor (*FC*).

The changes in the skeletal vibrational frequencies should result, theoretically, in a KIE of 1.02–1.22 (20, 32), whereas experimentally it was shown that H-bond-mediated ET has unity IE (30). The high KIE that we observed points to differences in the *FC* as the main cause. If this is the case, KIE is expected to increase markedly with decreasing temperature (20), because the FC temperature dependence saturates at low temperatures, because the frequency modes are "frozen." Indeed, our results are consistent with this prediction (Fig. 3*C* and *SI Text)*. "Freezing" of vibrational modes can be due to (*i*) quantum mechanical freezing, whereby high-frequency nuclear modes stop being thermally activated and tunneling becomes dominant, and (*ii*) thermodynamic freezing of the protein, whereby low-frequency structural modes freeze as the protein transitions to its glassy state (33, 34). In the next subsection we will discuss how the latter vibrational modes are consistent with our observation. We stress that freezing of the low-frequency structural modes also induces temperature-independent ETp, which is consistent with electronic tunneling. We further note that high KIE values have been commonly rationalized by the occurrence of proton-coupled electron transfer (35). However, this is unlikely in our system because we monitor DC currents with ion- (and, thus,

Table 1. H/D effects: solid state ETp vs. electrochemical ET

	Solid state			Solution*	
Parameter	Protium-labeled-Az	Deuterium-labeled-Az		Az in H_2O	Az in D_2O
E_a (meV)	0	$85_{@>180K}$	$0_{@<180K}$	530	560
KIE	$1.8_{@340K}$–$9.1_{@<180K}$			$0.65_{@280K}$–$0.84_{@315K}$	

*Taken from reference 15.

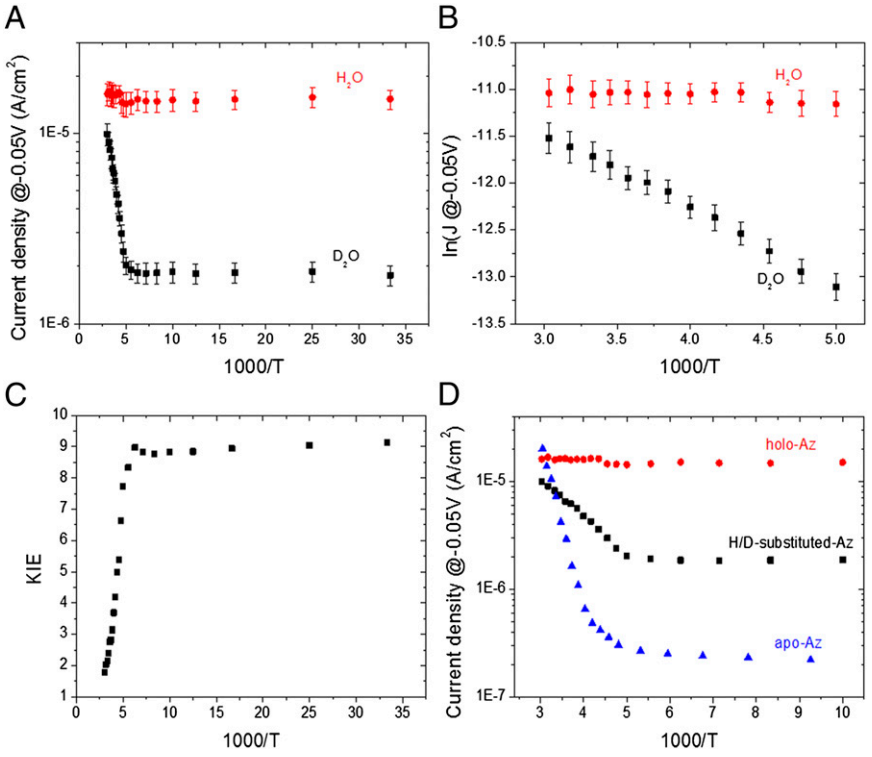

Fig. 3. ETp behavior. (*A*) Current density at −50 mV vs. inverse temperature of protium- and deuterium-labeled Az. (*B*) Zoom-in on the high-temperature part of *A* on a *ln*(J) scale. (*C*) Temperature dependence of the deuterium KIE. (*D*) Comparison between the effects of H/D substitution to the removal of Cu-ion (apo-Az).

proton-) blocking electrodes, without any signs of PT-induced polarization or hysteresis.

H/D-Induced Low-Frequency Modes in Az. The Az structure consists mainly of β-sheets, supported by an amide backbone H-bonding network. This provides a basis for rationalizing the KIE upon H/D exchange, as it should affect this network (2, 36, 37). Furthermore, altering the H-bonds in the Cu second coordination sphere was shown to cause marked changes in the protein's reduction potential (38). Such a change may reflect changes in protein flexibility, mainly around the Cu site (39–41), that could have two outcomes (42): (*i*) stiffer bonding may increase the protein's reorganization energy; or (*ii*) a less flexible protein has a shallower energy landscape of the (ET) reaction coordinate, which also alters the activation energy. In this context, in a recent NMR study (43) the presence of Cu was shown to increase the rigidity of the binding site of Az. We propose that such an increase enhances the ET (and in our study ETp) efficiency. Therefore, the difference in ETp temperature dependence between H- and D-labeled Az (Fig. 3) may result from the change in the structural vibrational modes of its β-sheets and/or the Cu coordination sphere. Although we cannot pinpoint the specific vibrational modes that are most affected by H/D exchange, we can speculate that a more flexible protein (i.e., deuterated Az) will have lower energy frequency modes, $\hbar\omega$, compared with the more rigid protium-Az, as shown both experimentally (44) and theoretically (45) for other proteins. Thus, in the high-temperature regime, the lower energy frequency modes of the deuterated Az may cause thermally activated ETp, if $\hbar\omega \leq 2k_BT$ (46). This is consistent with our observations: the 180 K transition temperature corresponds to $\hbar\omega = \sim 300$ cm^{-1}, which can be ascribed to the *FC*. Saturation of the KIE <180 K is consistent with freezing of these modes.

Advantages of Macroscopic Solid-State ETp Measurements. Our experimental approach allows high-sensitivity investigation of the role of intramolecular H-bonds (in ETp), while essentially excluding solvent effects. Moreover, this approach minimizes the chance that the measurement will cause a change in the protein conformation, because any minor structural changes would affect the ETp process, as we observed for bacteriorhodopsin (47). Thus, the temperature-independent ETp process via H-labeled Az excludes structural changes in the protein as a function of temperature up to its denaturation temperature.

The ability to measure at low temperatures enabled the present observation of an increase in KIE with decreasing temperature, a task that is extremely difficult with the common electrochemical approach for ET measurements via proteins. The solid-state experimental approach allows performance of measurements at such low temperatures and detection of current densities through the protein that are orders of magnitude smaller than what can be measured by nanoscopic (scanning probe-based) techniques, with instant spatial averaging of the current density. The observed KIE reflects the ability of the solid-state ETp approach to make reliable measurements of low current densities at low temperatures.

Conclusion

The results of our solid-state measurements allow excluding the effect of the bulk H_2O/D_2O solvent on the ETp rate, while focusing on the intramolecular differences caused by deuteration within the protein. We suggest that the relatively large KIE values that we find reflect a change in the protein flexibility, a change that may well be very hard to observe in an aqueous environment, where solvent effects can mask it. These results are consistent with a significant role of the H-bonding network of the mainly β-sheet structured Az in the solid-state ETp across it and support a through-(H-containing)-bond mechanism of ETp across proteins.

Materials and Methods

Protein Preparation. *Alcaligenes faecalis* Az was generously provided by R. P. Ambler (University of Edinburgh, Edinburgh, UK), and its isolation and purification procedures were as previously reported (48). The protocol of Farver et al. (15) was used for the deuteration process: the protonated Az (~1.5 mg) in 20 mM phosphate buffer at pH7 was diluted in a deuterated buffer containing 20 mM D_3PO_4 (D, 99% in 85% D_2O; Cambridge Isotope Laboratories) and 100 mM NaOD (D, 99.5% in 40% D_2O; Cambridge Isotope Laboratories) in D_2O (99.9%; Sigma-Aldrich) at ~pD7. The diluted solution was repeatedly (10 cycles) concentrated by Amicon Ultracell – 4k (Millipore), rediluted in the deuterated buffer, and left overnight. The final solution concentration for both of the protonated and deuterated samples was ~0.1 mM.

NMR Measurement. NMR samples contained ~1 mg Az dissolved in 90% H_2O/10% D_2O for the protium-labeled Az or 100% D_2O for the deuterium-labeled Az, in 20 mM NaH_2PO_4 or NaD_2PO_4 (pH 7.0). All NMR spectra were acquired on a Bruker AVIII800 NMR spectrometer equipped with TCI CryoProbe. One-dimensional ^{1}H NMR spectra and 2D homonuclear Hartmann-Hahn (HOHAHA) spectra (49, 50) were acquired at 303 K using excitation sculpting sequence (51) for water suppression. Mixing time used in the 2D-HOHAHA experiments was 80 ms. All spectra were processed and analyzed using Topspin (Bruker Biospin) software.

Spectroscopic Analysis. A ChirascanT Circular Dichroism Spectrometer (Applied Photophysics) was used for the CD analysis. A Cary 5000 UV-vis-NIR spectrophotometer (Varian, a part of Agilent Technologies) was used for the optical absorption measurements. A FluoroLog Modular Spectrofluorometer (Horiba Jobin Yvon) was used for the photoluminescence measurements. A rectangular quartz cuvettete with a path length of 3 mm was used for the CD and optical absorption measurements. A 5-mm diameter square quartz cuvettete was used for the photoluminescence measurements.

Surface Preparation. The protein monolayer surface was prepared as previously reported (11) with a few modifications: highly doped (<0.005 Ω cm) p-type Si surface <100> was cleaned by bath sonication in ethyl acetate/acetone/ethanol (2 min in each), followed by 30 min of piranha treatment (7/3 vol/vol of H_2SO_4/H_2O_2) at 80 °C. The Si surface was then thoroughly rinsed in Milli-Q (18 MΩ) water, dipped in 2% HF solution for 1.5 min, to etch the Si surface (leaving an Si-H surface), put in fresh piranha for ~5 s for controlled growth of a thin oxide layer (9–10 Å), and the surface was then immediately rinsed thoroughly in water and dried under a nitrogen stream. A monolayer of 3-mercaptopropyl trimethoxysilane (3-MPTMS, SH-terminated linker, 95%; Sigma-Aldrich) was prepared by immersing the SiO_2 substrate in 10 mM 3-MPTMS in bicyclohexyl for 1 h, followed by 3 min of bath sonication in acetone and 10 s in hot ethanol, yielding a monolayer thickness of ~7 Å. The 3-MPTMS coated surface was immersed in either the protonium-labeled Az solution (~1 mg/mL) or the deuterated Az in the deuterated buffer for 2 h, where the Az was covalently connected to the SH group of the linker via its cysteine (Cys26-Cys3) thiolate.

AFM Imaging. The topography of the self-assembled monolayer of proteins was characterized by AFM in tapping mode. A Solver P47 SPM system (NDMDT) and Si probes (NSC36, 75kHz, 0.6 N/m; MikroMasch) were used.

Current-Voltage Measurements. The back (InGa) and top (Hg) contacts were prepared and deposited as previously reported (11). The Hg was places on top of the protein monolayer by capillary. All of the results were obtained on macroscopic areas (~0.2-mm^2 contact area, containing 10^9–10^{10} protein molecules). The sample was placed in low vacuum (0.1 mbar) chamber in a TTPX cryogenic system (Lakeshore), and both the sample holder and the probes were cooled. The temperature was monitored and controlled with an accuracy of 0.2 K. Between each change in temperature the sample was not measured, so as to allow it to reach thermal equilibrium.

ACKNOWLEDGMENTS. We thank T. Scherf for assisting with the NMR measurements; M. Bixon, H. Gray, J. Jortner, A. Nitzan, and S. Skourtis for fruitful discussions; and the reviewers for helpful constructive criticism. This study was supported in part by the Minerva Foundation (Munich, Germany). N.A. received financial support from the Clore program. M.S. holds the Katzir-Makineni Chair in Chemistry. D.C. holds the Schaefer Chair in Energy Research.

1. Groeneveld CM, Canters GW (1988) NMR study of structure and electron transfer mechanism of *Pseudomonas aeruginosa* azurin. *J Biol Chem* 263(1):167–173.
2. Regan JJ, et al. (1995) Electron tunneling in azurin: The coupling across a beta-sheet. *Chem Biol* 2(7):489–496.
3. Farver O, Pecht I (2007) Elucidation of electron-transfer pathways in copper and iron proteins by pulse radiolysis experiments. *Prog Inorganic Chem* 55:1–78.
4. Gray HB, Winkler JR (2010) Electron flow through metalloproteins. *Biochim Biophys Acta Bioenerg* 1797(8):1563–1572.
5. Gray HB, Winkler JR (2003) Electron tunneling through proteins. *Q Rev Biophys* 36(3): 341–372.
6. Chi QJ, et al. (2000) Molecular monolayers and interfacial electron transfer of *Pseudomonas aeruginosa* azurin on Au(111). *J Am Chem Soc* 122(17):4047–4055.
7. Alessandrini A, Corni S, Facci P (2006) Unravelling single metalloprotein electron transfer by scanning probe techniques. *Phys Chem Chem Phys* 8(38):4383–4397.
8. Davis JJ, Wang N, Morgan A, Zhang TT, Zhao JW (2006) Metalloprotein tunnel junctions: Compressional modulation of barrier height and transport mechanism. *Faraday Discuss* 131:167–179, discussion 205–220.
9. Zhao JW, Davis JJ, Sansom MSP, Hung A (2004) Exploring the electronic and mechanical properties of protein using conducting atomic force microscopy. *J Am Chem Soc* 126(17):5601–5609.
10. Sepunaru L, Pecht I, Sheves M, Cahen D (2011) Solid-state electron transport across azurin: From a temperature-independent to a temperature-activated mechanism. *J Am Chem Soc* 133(8):2421–2423.
11. Ron I, et al. (2010) Proteins as electronic materials: Electron transport through solid-state protein monolayer junctions. *J Am Chem Soc* 132(12):4131–4140.
12. Beratan DN, Betts JN, Onuchic JN (1991) Protein electron transfer rates set by the bridging secondary and tertiary structure. *Science* 252(5010):1285–1288.
13. Antonello S, Formaggio F, Moretto A, Toniolo C, Maran F (2003) Anomalous distance dependence of electron transfer across peptide bridges. *J Am Chem Soc* 125(10):2874–2875.
14. Scullion L, et al. (2011) Large conductance changes in peptide single molecule junctions controlled by pH. *J Phys Chem C* 115(16):8361–8368.
15. Farver O, Zhang JD, Chi QJ, Pecht I, Ulstrup J (2001) Deuterium isotope effect on the intramolecular electron transfer in *Pseudomonas aeruginosa* azurin. *Proc Natl Acad Sci USA* 98(8):4426–4430.
16. Chi Q, Farver O, Ulstrup J (2005) Long-range protein electron transfer observed at the single-molecule level: In situ mapping of redox-gated tunneling resonance. *Proc Natl Acad Sci USA* 102(45):16203–16208.
17. Mei G, et al. (1996) Probing the structure and mobility of *Pseudomonas aeruginosa* azurin by circular dichroism and dynamic fluorescence anisotropy. *Protein Sci* 5(11): 2248–2254.
18. Schnyder B, Kotz R, Alliata D, Facci P (2002) Comparison of the self-chemisorption of azurin on gold and on functionalized oxide surfaces. *Surf Interface Anal* 34(1):40–44.
19. Vilan A, Cahen D (2002) Soft contact deposition onto molecularly modified GaAs. Thin metal film flotation: Principles and electrical effects. *Adv Funct Mater* 12(11-12):795–807.
20. Buhks E, Bixon M, Jortner J (1981) Deuterium isotope effects on outer-sphere electron-transfer reactions. *J Phys Chem* 85(25):3763–3766.
21. Hirst J, Ackrell BAC, Armstrong FA (1997) Global observation of hydrogen/deuterium isotope effects on bidirectional catalytic electron transport in an enzyme: Direct measurement by protein-film voltammetry. *J Am Chem Soc* 119(32):7434–7439.
22. Shafirovich V, Dourandin A, Geacintov NE (2001) Proton-coupled electron-transfer reactions at a distance in DNA duplexes: Kinetic deuterium isotope effect. *J Phys Chem B* 105(35):8431–8435.
23. Muller N (1991) Model calculations of changes of thermodynamic variables for the transfer of nonpolar solutes from water to water-d2. *J Solution Chem* 20(7):669–680.
24. Ben-naim A, Marcus Y (1984) Solvation thermodynamics of nonionic solutes. *J Chem Phys* 81(4):2016–2027.
25. Marcus Y, Ben-naim A (1985) A study of the structure of water and its dependence on solutes, based on the isotope effects on solvation thermodynamics in water. *J Chem Phys* 83(9):4744–4759.
26. Brunschwig BS, Ehrenson S, Sutin N (1986) Solvent reorganization in optical and thermal electron-transfer processes. *J Phys Chem* 90(16):3657–3668.
27. Zhang X, Yang H, Bard AJ (1987) Variation of the heterogeneous electron-transfer rate constant with solution viscosity: reduction of aqueous solutions of [(EDTA) chromium(III)]-at a mercury electrode. *J Am Chem Soc* 109(7):1916–1920.
28. Vidulich GA, Evans DF, Kay RL (1967) The dielectric constant of water and heavy water between 0 and 40.degree. *J Phys Chem* 71(3):656–662.
29. Horng ML, Gardecki JA, Papazyan A, Maroncelli M (1995) Subpicosecond measurements of polar solvation dynamics—coumarin-153 revisited. *J Phys Chem* 99(48): 17311–17337.
30. Pal H, Nagasawa Y, Tominaga K, Yoshihara K (1996) Deuterium isotope effect on ultrafast intermolecular electron transfer. *J Phys Chem* 100(29):11964–11974.
31. Roberts JA, Kirby JP, Nocera DG (1995) Photoinduced electron transfer within a donor-acceptor pair juxtaposed by a salt bridge. *J Am Chem Soc* 117(30):8051–8052.
32. Buhks E, Bixon M, Jortner J, Navon G (1981) Quantum effects on the rates of electron-transfer reactions. *J Phys Chem* 85(25):3759–3762.
33. Teeter MM, Yamano A, Stec B, Mohanty U (2001) On the nature of a glassy state of matter in a hydrated protein: Relation to protein function. *Proc Natl Acad Sci USA* 98(20):11242–11247.
34. Ringe D, Petsko GA (2003) The 'glass transition' in protein dynamics: What it is, why it occurs, and how to exploit it. *Biophys Chem* 105(2-3):667–680.

35. Hammes-Schiffer S (2001) Theoretical perspectives on proton-coupled electron transfer reactions. *Acc Chem Res* 34(4):273–281.
36. McDougall AO, Long FA (1962) Relative hydrogen bonding of deuterium. II. Acid ionization constants in H_2O and D_2O. *J Phys Chem* 66(3):429–433.
37. Calvin M, Hermans JJ, Scheraga HA (1959) Effect of deuterium on the strength of hydrogen bonds. *J Am Chem Soc* 81(19):5048–5050.
38. Marshall NM, et al. (2009) Rationally tuning the reduction potential of a single cupredoxin beyond the natural range. *Nature* 462(7269):113–116.
39. Benning MM, Meyer TE, Rayment I, Holden HM (1994) Molecular structure of the oxidized high-potential iron-sulfur protein isolated from *Ectothiorhodospira vacuolata*. *Biochemistry* 33(9):2476–2483.
40. Palfey BA, Basu R, Frederick KK, Entsch B, Ballou DP (2002) Role of protein flexibility in the catalytic cycle of p-hydroxybenzoate hydroxylase elucidated by the Pro293Ser mutant. *Biochemistry* 41(26):8438–8446.
41. Battistuzzi G, Borsari M, Cowan JA, Ranieri A, Sola M (2002) Control of cytochrome C redox potential: Axial ligation and protein environment effects. *J Am Chem Soc* 124(19):5315–5324.
42. Marcus RA (2007) H and other transfers in enzymes and in solution: Theory and computations, a unified view. 2. Applications to experiment and computations. *J Phys Chem B* 111(24):6643–6654.
43. Zaballa ME, Abriata LA, Donaire A, Vila AJ (2012) Flexibility of the metal-binding region in apo-cupredoxins. *Proc Natl Acad Sci USA* 109(24):9254–9259.
44. Whitmire SE, et al. (2003) Protein flexibility and conformational state: A comparison of collective vibrational modes of wild-type and D96N bacteriorhodopsin. *Biophys J* 85(2):1269–1277.
45. Kovacs JA, Chacón P, Abagyan R (2004) Predictions of protein flexibility: First-order measures. *Proteins* 56(4):661–668.
46. Marcus RA, Sutin N (1985) Electron transfers in chemistry and biology. *Biochim Biophys Acta* 811(3):265–322.
47. Sepunaru L, Friedman N, Pecht I, Sheves M, Cahen D (2012) Temperature-dependent solid-state electron transport through bacteriorhodopsin: Experimental evidence for multiple transport paths through proteins. *J Am Chem Soc* 134(9):4169–4176.
48. Rosen P, Segal M, Pecht I (1981) Electron transfer between azurin from *Alcaligenes faecalis* and cytochrome c551 from *Pseudomonas aeruginosa*. *Eur J Biochem* 120(2): 339–344.
49. Braunschweiler L, Ernst RR (1983) Coherence transfer by isotropic mixing: Application to proton correlation spectroscopy. *J Magn Reson* 53(3):521–528.
50. Rucker SP, Shaka AJ (1989) Broadband homonuclear cross polarization in 2D NMR using DIPSI-2. *Mol Phys* 68(2):509–517.
51. Hwang TL, Shaka AJ (1995) Water suppression that works. Excitation sculpting using arbitrary wave-forms and pulsed-field gradients. *J Magn Reson A* 112(2):275–279.